A statistical analysis of the capabilities of LA-ICPMS as a prospective geochronology instrument for Rb-Sr dating

Ari Cacopardo

GEOLOGY 394

April 28th, 2020

Advisors: Drs. R. Arévalo, R. D. Ash, and W. F. McDonough

Abstract

The goal of this study is to evaluate statistically the potential for using LA-ICPMS (laser ablation – inductively coupled plasma mass spectrometry) technology to determine accurate and precise absolute ages of geological samples isolated on planetary bodies in the solar system via an *in situ* Rb-Sr geochronometer. The 2015 NASA Technology Roadmap establishes performance goals for advanced instrumentation to provide *in situ* radiometric age determinations with an analytical uncertainty of ±400 million years (2 standard deviations) or better for a sample having an age between 1 – 4 Ga on the surface of remote solar system bodies. With this quantitative constraint, the temporal evolution of planetary surfaces can be documented and provide a fundamental calibration scale for crater counting versus age studies on bodies in the solar system.

This research identifies the analytical challenges facing Rb-Sr chronological studies, including quantifying contributions from isobaric interferences (e.g., Kr isotopes, doubly charged REE, Ca dimers/argides, Zn oxides and Sc argides) on relevant masses as a function of sample chemistry. Using a suite of standard reference materials, isotopic fractionation processes incurred by LA-ICPMS analyses are characterized and corrected for using a well-established exponential law. Based on empirical data, isobaric interferences are modeled and corrected for, with the goal of accurately identifying uncertainties in $^{87}Sr/^{86}Sr$ and $^{87}Rb/^{86}Sr$ measurements, and by extension inferred age of investigated samples.

A range of experimental procedures have been developed that maximize the accuracy and precision of the isotopic abundance measurements for samples, based on the analysis of basaltic reference glasses (i.e., BIR-1G and BHVO-2G). Here, $^{87}Sr/^{86}Sr$ and $^{87}Rb/^{86}Sr$ values have been determined for BIR-1G and BHVO-2G with an external reproducibility of 1.6% and 6%, (2σ) respectively and an accuracy of 0.7% and 14%, respectively, relative to preferred published values. Varying the operating parameters of the laser, such as spot size and dwell times have been explored to attain these figures. Future analytical targets to be refined, to reach the greatest accuracy and precision performance metrics, are identified.

Introduction

This study critically evaluates the capabilities of LA-ICPMS as a chronological tool, specifically adapted to exploit the Rb-Sr isochron system. The goal here is to: i) identify and quantify contributions of problematic isobaric interferences that statistically impact the inferred $^{87}Sr/^{86}Sr$ ratio; ii) establish analytical methods that minimize isobar production rates and maximize sensitivity to Rb and Sr; iii) test different computational techniques for correcting isobaric interferences and instrumental induced mass fractionation; and, iv) determine the levels of accuracy and precision that can be obtained for absolute ages of basalt, the most pervasive lithology observed on Mars (Ehlmann and Edwards 2014).

Motivation

Having the capability of determining radiometric ages on the surface of Mars (or other solar system bodies) will significantly advance our current understanding of the timing of formative events in the history of the red planet. Currently, the primary method of estimating absolute ages of planetary surfaces in the solar system is crater counting (relative ages are inferred based on first order geological principles, such as cross-cutting relationships). Simply

put, the older the surface, the more craters there are. This method is based on a calibration rate from radiometrically dated samples from the moon and a modeled impactor flux, with significant variances between different published models (Robbins 2014). As a result, there are large uncertainties associated with estimated geologic ages on Mars. By evaluating the capabilities of LA-ICPMS as a geochronology instrument, a case can be made for adapting LA-ICPMS for *in situ* measurements on Mars.

Why Rb-Sr via LA-ICPMS?

LA-ICPMS hardware/techniques offer an opportunity to analyze multiple minerals in a single sample and generate a closed system isochron. Such methods require minimal sample preparation. Importantly, B. Farcy and others have been developing a miniaturized instrument with reduced mass/volume/power resources requirements for spaceflight application. The Rb-Sr isotopic system is widely used in chronological studies of material in the solar system due to its long half-life (49.2 Gyr). Cohen et. al 2019 overviews the other viable *in situ* chronology instrumentation and isotopic systems (K-Ar, Pb-Pb, and secondary ionization for Rb-Sr).

Background

Rb-Sr decay

The Rb-Sr radiometric system enables the determination of the absolute age of formation or alteration of a rock. The system being evaluated is the beta decay of ^{87}Rb per the following relationship:

$$^{87}_{37}Rb \rightarrow {}^{87}_{38}Sr + \beta^- + \overline{\nu} + Q,$$

where β^- represents an ejected electron, $\overline{\nu}$, an antineutrino, and Q released heat. The half-life for this reaction is 49.2 billion years (Dickin 2005). Radiometric dating consists of measuring the abundance of the daughter isotope produced from radiogenic decay of the parent isotope and comparing these isotopes abundances to those of a naturally occurring, stable isotope of the daughter element. The initial quantity of the daughter isotope that was inherited prior to the closure of the system, with respect to Rb and Sr, needs to be considered. The decay equation for Rb-Sr is:

$$^{87}Sr_p = {}^{87}Sr_i + {}^{87}Rb \times (e^{\lambda t} - 1)$$

where $^{87}Sr_i$ is the initial abundance of the isotope, $^{87}Sr_p$ is the present-day abundance, λ is the decay constant, and is equal to $\ln(2)/t_{1/2}$, and t is time since closure to diffusion. Dividing the above equation by the stable isotope, ^{86}Sr, results is an easier and more precise method to determine the age, because high precision ratios are more readily measured via mass spectrometry than absolute abundances. The resulting equation is:

$$\frac{^{87}Sr}{^{86}Sr}_p = \frac{^{87}Sr}{^{86}Sr}_i + \frac{^{87}Rb}{^{86}Sr} \times (e^{\lambda t} - 1)$$

(Dickin 2005). This equation has the form y=b +xm, where the initial (^{87}Sr/^{86}Sr) represents the y-intercept value, (^{87}Rb/^{86}Sr) represents the x-axis value. Thus, an isochron results from plotting a series of (^{87}Sr/^{86}Sr) and (^{87}Rb/^{86}Sr) ratios in a closed system suite of cogenetic minerals, documenting the sample's formation age. The uncertainty in the age derived from such an

isochron reflects errors propagated from 1) isobaric interference subtractions, 2) mass fractionation corrections outlined further below, 3) the spread in Rb/Sr observed in a sample (or variance in x-axis), 4) the fit of linear regression analysis, and 5) statistical scatter.

Laser Ablation Inductively Coupled Plasma Mass Spectrometry

A traditional LA-ICPMS instrument includes a pulsed UV laser system and a quadrupole or sector field mass spectrometer. Mass spectrometers (MS) have three fundamental components: source, mass analyzer, and detector. A typical LA-ICPMS experiment begins by irradiating the surface of a sample within the ablation chamber (LA). A focused beam of pulsed UV-wavelength photons is coupled to a sample, which results in an explosive ablation plume of fine particles, with a particle mode of ~50 nanometers in diameter (Arevalo 2014). Helium gas is used to transport these particles to the source of the MS, which is an argon based inductively coupled plasma (ICP). This argon gas plasma atomizes and ionizes the ablated material with ions extracted into the mass analyzer via vacuum and high voltage potentials. After separation of the ion from the electrons via a grounding plate, the ions are focused via a suite of ion optical lenses, and then separated by their respective mass-to-charge ratios (m/z) by a controlled magnetic field, followed by an electrostatic analyzer (reverse Nier Johnson geometry). Ions are detected by a secondary electron multiplier and counted and processed (Olesik 2014). LA-ICPMS allows for spatially resolved elemental and isotopic analyses, enabling multiple minerals in a single sample to be readily analyzed independently (Jenner and Arevalo 2016), potentially leading to the generation of an isochron.

A baseline test of Rb-Sr geochronology via LA-ICPMS has been conducted to determine the level of accuracy and precision that can be obtained using the instrumentation at the University of Maryland. Along with the baseline test, IsoplotR, an online software package, was used to investigate the required spread of $^{87}Rb/^{86}Sr$ ratios to build an isochron yielding the desired age error (±400 Myr). Based on Martian mineralogy, the necessary $^{87}Rb/^{86}Sr$ spread will be compared to expected $^{87}Rb/^{86}Sr$ ratios to determine whether an accurate isochron will be feasible.

Working Hypothesis

The achievable accuracy and precision for Rb-Sr dating via LA-ICPMS as a planetary chronology instrument will be within the desired standards set by NASA, specifically ± 400 million years (2 standard deviations) on a sample age between 1 – 4 Ga.

Methodology

Isobaric Interferences

The isobaric interferences that affect the desired ratios are isotopes of Kr, doubly charged rare earth elements (REE), Ca dimers and argides, and Zn oxides (Table 1). Krypton is introduced to the system from the Ar that feeds the plasma source, and the He that carries the ablated aerosols into the ICPMS; ^{84}Kr and ^{86}Kr interfere with measurements of ^{84}Sr and ^{86}Sr, repsectively. Doubly charged REE, such as $^{168}Er^{2+}$, $^{170}Yb^{2+}$, $^{172}Yb^{2+}$, $^{174}Yb,^{2+}$, and $^{176}Lu^{2+}$, may interfere with measurements of ^{84}Sr, ^{85}Rb, ^{86}Sr, $^{87}Sr + ^{87}Rb$, ^{88}Sr, respectively, if their abundances are sufficently high (depending on the production rate of REE^{2+}/REE^{+}). Calcium dimers (e.g., $^{42}Ca^{42}Ca^{+}$) and argides (e.g., $^{46}Ca^{40}Ar^{+}$) interfere with masses of interest between 83 – 88, particularly in samples with high Ca/Sr ratios (Jochum et al., 2009). Other oxides and argides,

such as $^{68}Zn^{16}O^{+}$ and $^{45}Sc^{40}Ar^{+}$, can also interfere in the desired mass range. However, the production rates of all of these doubled-charged and molecular isobars need to be quantified as a function of sample chemistry and analytical conditions in order to determine their relative impact for Rb-Sr chronology.

Source of Interference Mass	82	83	84	85	86	87	88
Strontium	-	-	^{84}Sr	-	^{86}Sr	^{87}Sr	^{88}Sr
Krypton	^{82}Kr	^{83}Kr	^{84}Kr	-	^{86}Kr	-	-
Rubidium	-	-	-	^{85}Rb	-	^{87}Rb	-
Zinc Oxides	-	$^{66}Zn^{17}O$	$^{68}Zn^{16}O$	$^{68}Zn^{17}O$	$^{68}Zn^{18}O$	$^{70}Zn^{17}O$	$^{70}Zn^{18}O$
	-	$^{67}Zn^{16}O$	-	-	$^{70}Zn^{16}O$	-	-
Calcium Dimers	-	$^{40}Ca^{43}Ca$	$^{40}Ca^{44}Ca$	$^{42}Ca^{44}Ca$	$^{40}Ca^{46}Ca$	$^{43}Ca^{44}Ca$	$^{40}Ca^{48}Ca$
	-	-	-	-	$^{42}Ca^{44}Ca$	-	$^{42}Ca^{48}Ca$
	-	-	-	-	$^{43}Ca_2$	-	$^{42}Ca^{46}Ca$
	-	-	-	-	-	-	$^{44}Ca_2$
Calcium Argides	-	$^{43}Ca^{40}Ar$	$^{48}Ca^{36}Ar$	-	$^{48}Ca^{38}Ar$	-	$^{48}Ca^{40}Ar$
	-	-	$^{46}Ca^{38}Ar$	-	$^{46}Ca^{40}Ar$	-	-
	-	-	$^{44}Ca^{40}Ar$	-	-	-	-
Doubly Charged REE	^{164}Er	^{166}Er	^{168}Yb	^{170}Yb	^{172}Yb	^{174}Yb	^{176}Yb
	^{164}Dy	-	^{168}Er	^{170}Er	-	-	^{176}Hf
	-	-	-	-	-	-	^{176}Lu

Table 1: Sources of interference in desired mass range (Vroon et al., 2008).

Mass Fractionation

Another factor that can affect the accuracy of LA-ICPMS measurements is mass fractionation, or the disproportionate transmission of heavy ions relative to light ions due to light ions being deflected more than heavier ions, resulting in a measured isotopic ratio that does not reflect the true ratio of the sample. This fractionation may be corrected for by the exponential law:

$$R_c = R_m \times (m_1/m_2)^{\alpha}$$

where R_c is the corrected ratio, R_m is the measured ratio, (m_1/m_2) is the ratio of isotopic masses, and α is the "alpha" value. Alpha is calculated from an isotope pair known to remain constant in geological materials by:

$$\alpha = \ln(R_m/R_t)/\ln(m_1/m_2)$$

where R_t is the true ratio of the isotopes.

BIR-1G and BHVO-2G Analyses

The standard reference materials BIR-1G and BHVO-2G were analyzed using LA-ICPMS as a feasibility demonstration for the broader objectives of this study, statistically assessing the capabilities of LA-ICPMS instrumentation as an *in situ* chronology instrument. BIR-1G and BHVO-2G are basaltic reference glasses with Sr abundances of 110 μg g^{-1} and 395 μg g^{-1}, respectively, and Rb abundances of 0.215 μg g^{-1} and 9 μg g^{-1}, respectively (Jochum et al., 2007).

The laser system used was a New Wave UP213; the native wavelength produced by this NdYAG laser (1064nm) passes through a series of frequency multiplying crystals to produce 213nm wavelength radiation. This system was coupled to a Thermo-Finnigan Element 2 ICPMS. The relevant operating parameters for the analyses can be found in Table 2 and 3.

Laser	
Spot size	100 μm
Repetition rate	7 Hz
Fluence	2.5-4.0 J cm^{-2}

Table 2: New Wave UP213 operating parameters.

ICPMS	
Power	1270 W
Cool gas (Ar)	16 L min^{-1}
Auxiliary gas (Ar)	1.05 L min^{-1}
Sample gas (Ar)	0.735 L min^{-1}
Ablation gas (He)	0.735 L min^{-1}
Extraction voltage	-2000V

Table 3: Element 2 operating parameters.

The element menu for the experiment consisted of: ^{77}Se, ^{78}Se, ^{82}Kr, ^{83}Kr, ^{84}Sr, ^{85}Rb, ^{86}Sr, ^{87}Sr, ^{88}Sr. These isotopes were measured for 10 ms per scan (nominally), with a mass window of one and one sample per peak (see Appendices). Selenium was analyzed to check for interference of ^{82}Se on ^{82}Kr; it was determined there was no interference for the samples investigated. Krypton was analyzed to correct for the interference of ^{84}Kr and ^{86}Kr on ^{84}Sr and ^{86}Sr.

BIR-1G and BHVO-2G were analyzed on two separate occasions; first in November 2019 and then again in January 2020. The November analyses utilized a 100 μm spot size and 10 ms dwell time. The correction method for November follows:

1st Correction Method

Krypton

$$^{84}\text{Mass} - {}^{88}\text{Sr} \times \left(^{84}\text{Sr}/^{88}\text{Sr}\right)_{\text{true}} = {}^{84}\text{Kr}_{\text{calculated}}$$
$$^{84}\text{Kr}_{\text{calculated}} \times \left(^{86}\text{Kr}/^{84}\text{Kr}\right)_{\text{true}} = {}^{86}\text{Kr}_{\text{calculated}}$$
$$^{84}\text{Mass} - {}^{84}\text{Kr}_{\text{calculated}} = {}^{84}\text{Sr}_{\text{calculated}}$$
$$^{86}\text{Mass} - {}^{86}\text{Kr}_{\text{calculated}} = {}^{86}\text{Sr}_{\text{calculated}}$$
Estimated $^{84}Sr/^{86}Sr$ and $^{86}Sr/^{88}Sr$

Rubidium

$$^{85}\text{Rb}_{\text{measured}} \times \left(^{87}\text{Rb}/^{85}\text{Rb}\right)_{\text{true}} = {}^{87}\text{Rb}_{\text{calculated}}$$
$$^{87}\text{Sr}_{\text{measured}} - {}^{87}\text{Rb}_{\text{calculated}} = {}^{87}\text{Sr}_{\text{calculated}}$$
Estimated $^{87}Sr/^{86}Sr$

Mass Fractionation – Alpha

$$\text{Alpha} = \frac{Ln\left(\frac{^{86}}{^{88}}Sr\ True \Big/ \frac{^{86}}{^{88}}Sr\ Measured\right)}{Ln\frac{88}{86}}$$

$^{87}Sr/^{86}Sr_{estimated} \times (86/88)^{\alpha} = {}^{87}Sr/^{86}Sr_{corrected}$

$^{87}Sr_{measured} - {}^{87}Rb_{corrected} = {}^{87}Sr_{corrected}$

Corrected $^{87}Sr/^{86}Sr$

The exponential law, $R_c = R_m \times (m_1/m_2)^{\alpha}$, was used to correct for mass fractionation by using the measured $^{88}Sr/^{86}Sr$ ratio. The 2 standard error of the mean (SEM) uncertainties were calculated by:

$$\frac{2SD}{\sqrt{n}}$$

where SD is the standard deviation of the average signal and n is the number of data points. The canonical ratios are; ($^{84}Sr/^{88}Sr$) = 0.0068, ($^{86}Kr/^{84}Kr$) = 0.3035, ($^{87}Rb/^{85}Rb$) = 0.3865 (IUPAC Technical Report 2013).

The January analyses recreated the previous conditions as well as varying two operating parameters of the laser system: the laser spot size expanded to 150 μm, and the dwell time increased to 50 ms. The 1st correction method (described above) was applied to all January analyses. Three other correction methods (outlined below) were explored for January analyses as well. These methods involve applying a mass fractionation correction during the krypton subtraction and different ways to correct the krypton inference. Interference from krypton presents the largest impact on the accuracy of the ratios due to relatively high-count rates (i.e., $\geq 10^3$ counts/s), most notably ^{86}Kr. The following correction methods were derived to explore the possible permutations of correcting for the various interferences.

2nd Method

Krypton

$^{84}\text{Mass} - {}^{88}Sr \times ({}^{84}Sr/{}^{88}Sr)_{true} = {}^{84}Kr_{calculated}$

$$\text{Alpha} = \frac{Ln\left(\frac{^{82}}{^{83}}Kr\ True \Big/ \frac{^{82}}{^{83}}Kr\ Measured\right)}{Ln\frac{82}{83}}$$

$^{86}Kr/^{83}Kr_{estimated} \times (82/83)^{\alpha} = {}^{86}Kr/^{83}Kr_{corrected}$

$^{86}Kr/^{83}Kr_{corrected} \times {}^{83}Kr_{measured} = {}^{86}Kr_{corrected}$

$^{86}\text{Mass} - {}^{86}Kr_{corrected} = {}^{86}Sr_{calculated}$

Estimated $^{86}Sr/^{88}Sr$

Rubidium

$^{85}Rb_{measured} \times ({}^{87}Rb/{}^{85}Rb)_{true} = {}^{87}Rb_{calculated}$

$^{87}Sr_{measured} - {}^{87}Rb_{calculated} = {}^{87}Sr_{calculated}$

Estimated $^{87}Sr/^{86}Sr$

Mass Fractionation – Alpha

$$\text{Alpha} = \frac{Ln\ {}^{\frac{86}{88}Sr\ True}\Big/_{\frac{86}{88}Sr\ Measured}}{Ln\frac{88}{86}}$$

$^{87}Sr\ /^{86}Sr_{estimated}$ x $(86/88)^{\alpha} = {}^{87}Sr\ /^{86}Sr_{corrected}$

$^{87}Sr_{measured} - {}^{87}Rb_{corrected} = {}^{87}Sr_{corrected}$

Corrected $^{87}Sr/^{86}Sr$

3rd Method

Krypton

Avg. $^{86}Kr_{background} - {}^{86}Mass = {}^{86}Sr_{estimated}$

Estimated $^{86}Sr/^{88}Sr$

Rubidium

$^{85}Rb_{measured}$ x $(^{87}Rb/^{85}Rb)_{true} = {}^{87}Rb_{calculated}$

$^{87}Sr_{measured} - {}^{87}Rb_{calculated} = {}^{87}Sr_{calculated}$

Estimated $^{87}Sr/^{86}Sr$

Mass Fractionation – Alpha

$$\text{Alpha} = \frac{Ln\ {}^{\frac{86}{88}Sr\ True}\Big/_{\frac{86}{88}Sr\ Measured}}{Ln\frac{88}{86}}$$

$^{87}Sr\ /^{86}Sr_{estimated}$ x $(86/88)^{\alpha} = {}^{87}Sr\ /^{86}Sr_{corrected}$

$^{87}Sr_{measured} - {}^{87}Rb_{corrected} = {}^{87}Sr_{corrected}$

Corrected $^{87}Sr/^{86}Sr$

4th Method

Krypton

Measured $^{86}Kr/^{83}Kr_{background}$

$$\text{Alpha} = \frac{Ln\ {}^{\frac{82}{83}Kr\ True}\Big/_{\frac{82}{83}Kr\ Measured}}{Ln\frac{82}{83}}$$

$^{86}Kr/^{83}Kr_{background} * (82/83)^{\alpha} = {}^{86}Kr\ /^{83}Kr_{corrected\text{-}background}$

$^{86}Kr\ /^{83}Kr_{corrected\text{-}background}$ x $^{83}Kr_{avg\text{-}counts} = {}^{86}Kr_{corrected}$

$^{86}Mass - {}^{6}Kr_{corrected} = {}^{86}Sr_{estimated}$

Estimated $^{86}Sr/^{88}Sr$

Rubidium

$^{85}Rb_{measured}$ x $(^{87}Rb/^{85}Rb)_{true} = {}^{87}Rb_{calculated}$

$^{87}Sr_{measured} - {}^{87}Rb_{calculated} = {}^{87}Sr_{calculated}$

Estimated $^{87}Sr/^{86}Sr$

Mass Fractionation – Alpha

$$\text{Alpha} = \frac{Ln\left(\frac{86}{88}Sr\ True \Big/ \frac{86}{88}Sr\ Measured\right)}{Ln\frac{88}{86}}$$

$^{87}Sr/^{86}Sr_{estimated} \times (86/88)^{\alpha} = {}^{87}Sr/^{86}Sr_{corrected}$

$^{87}Sr_{measured} - {}^{87}Rb_{corrected} = {}^{87}Sr_{corrected}$

Corrected $^{87}Sr/^{86}Sr$

Results

Element Solutions

The production rates of isobaric interferences, and the magnitude of mass dependent fractionation, were initially investigated using the ICPMS in solution mode. Single element solutions of Sc, Ca, Zn, Sr, 1:1 Sr and Rb, Yb and Ho were prepared by diluting 1000 ppm stock solutions by a dilution factor of 100, two times with 5% HNO_3 to reach the desired ppb level concentrations. The analysis of the Sc solution informed on the rate of argide production, Ca for dimer production, Zn for oxides, and Yb for doubly charged REE production, all prospective isobars on the mass stations required to determine $^{87}Sr/^{86}Sr$ and $^{87}Rb/^{86}Sr$. The Sr and 1:1 Rb-Sr solutions were analyzed to explore mass fractionation effects and the propagation of error when subtracting the contribution of ^{87}Rb from the net signal measured at mass 87. For each solution, the natural isotopes and the associated interfering mass numbers were analyzed. The $^{87}Sr/^{86}Sr$ ratio for the two Sr solutions were calculated by correcting for mass fractionation using the exponential law (Table 4).

Solution	Alpha	STD 1σ	% RSD	$^{87}Sr/^{86}Sr$	1 SEM	% RSD
Sr only	2.80	2.96	98.4%	0.698	0.043	6.2%
1:1 Rb-Sr	2.55	2.78	100.8%	0.608	0.153	25.1%

Table 4: Statistics of element solution experiments.

The production rates of doubly charged REE from Yb and Ho had an average doubly charged ion production rate of 0.15% (Table 3). Ho was used because it is monoisotopic. The data from the Sr and 1:1 Rb and Sr solutions were processed, and the $^{87}Sr/^{86}Sr$ ratios were calculated. For each pass on the ICPMS, approximately every 5 ms, a corrected $^{87}Sr/^{86}Sr$ ratio was calculated and plotted (Figure 1a and 1b). The accepted ratio is equal to 0.7031.

Isotope	1^+	2^+	$2^+/1^+$
^{171}Yb	1,200,000	950	0.08%
^{172}Yb	1,835,000	4,700	0.26%
^{173}Yb	1,350,000	925	0.07%
^{174}Yb	2,654,000	4260	0.16%
^{165}Ho	4,230,000	7540	0.18%

Table 3: Production rates for single element solutions of Yb and Ho.

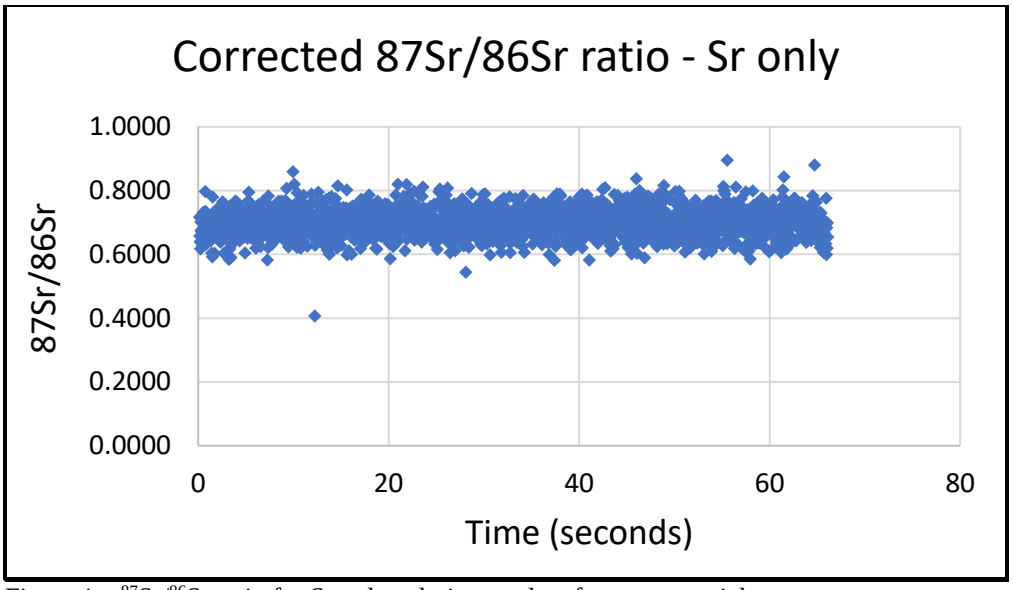

Figure 1a: $^{87}Sr/^{86}Sr$ ratio for Sr only solution mode reference material.

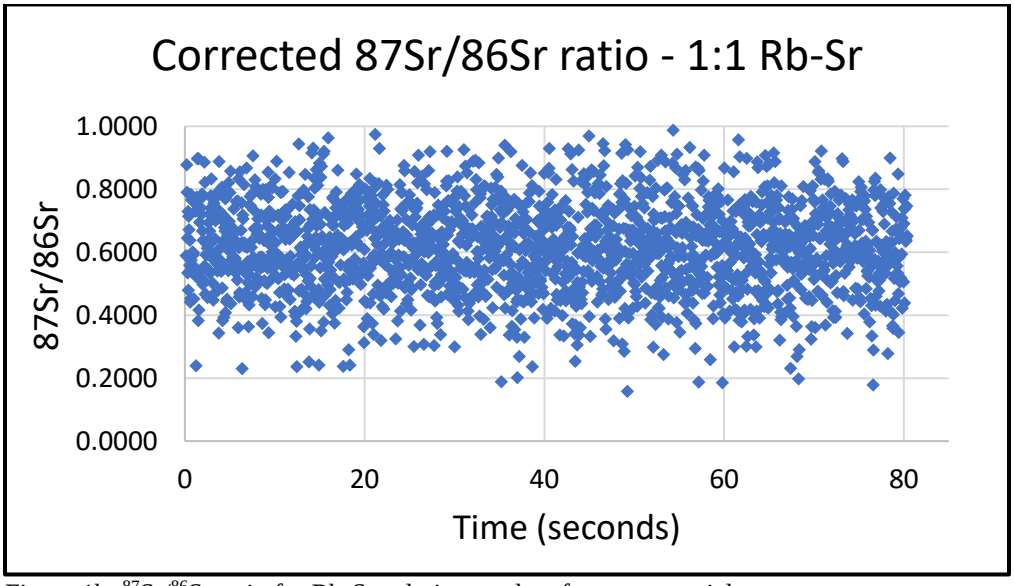

Figure 1b: $^{87}Sr/^{86}Sr$ ratio for Rb-Sr solution mode reference material.

Solid Sample Analyses

Plasma conditions (gas temperatures, electron densities, etc.) vary as a function of analyte introduction, thus wet chemical analyses may incur different isobar production rates and fractionation effects when compared to dry plasma analyses (LA). In order to increase the fidelity of the experiments, I analyzed a series of solid samples with the same overarching goals. The solids samples analyzed via LA-ICPMS were willemite (zinc silicate), thortveitite (scandium silicate), andradite (garnet – high calcium) and zircon (high REE). A ratio of the potential isobars to Rb or Sr (counts per second) were calculated based on the respective production rates for each isobar. If the measured isobaric production (counts per second) on the mass signal fell below a threshold ratio, then the effect of the isobar was deemed negligible. These samples contained

high abundances of the relevant isobars and low Rb and Sr concentrations, thus allowing for the identification of representative production rates.

The data from the Willemite for zinc oxides was complicated due to multiple interferences on the relevant mass signals; this data set is not further considered here given these complexities. The thortveitite produced a production rate of scandium argides of 0.01%. The andradite produced a production rate of calcium dimers (specifically $^{44}Ca^{44}Ca$) of 0.004%. The zircon produced a range of production rates for doubly charged REE from 10% to 0.5%, decreasing systematically as a function of increasing atomic mass (Table 5).

Isotope	1^+	2^+	$2^+/1^+$	Isotope	1^+	2^+	$2^+/1^+$
^{139}La	24500	3000	12.2%	^{159}Tb	9000	315	3.5%
^{140}Ce	216000	29000	13.4%	^{163}Dy	33000	1400	4.2%
^{141}Pr	9000	1100	12.2%	^{165}Ho	50000	1700	3.4%
^{146}Nd	6000	700	11.7%	^{166}Er	91000	2130	2.3%
^{147}Sm	2000	175	8.8%	^{169}Tm	79000	2100	2.7%
^{153}Eu	3250	270	8.3%	^{174}Yb	337000	9000	2.7%
^{157}Gd	3500	140	4.0%	^{175}Lu	121000	500	0.4%

Table 5: REE production rates zircon analyses.

BIR-1G and BHVO-2G

The standard reference materials BIR-1G and BHVO-2G were analyzed via LA-ICPMS as a feasibility assessment for this project. The accuracy of $^{87}Sr/^{86}Sr$ ratios for the November and January analyses of BIR-1G and BHO-2G are plotted in Figures 2a and 2b. Figures 3 and 4 show the different operating parameters varied. Figures 5a and b show the $^{87}Rb/^{86}Sr$ ratios for the January analyses. All ratios were corrected for krypton isobars and mass fractionation. The orange line represents the GeoRem (http://georem.mpch-mainz.gwdg.de/sample_query_pref.asp) preferred value for the $^{87}Sr/^{86}Sr$ ratio or $^{87}Rb/^{86}Sr$. The preferred values for BIR-1G are $^{87}Sr/^{86}Sr$ = 0.7031 and or $^{87}Rb/^{86}Sr$ = 0.0051**.** For BHVO-2G, $^{87}Sr/^{86}Sr$ = 0.7035 and $^{87}Rb/^{86}Sr$ = 0.0656

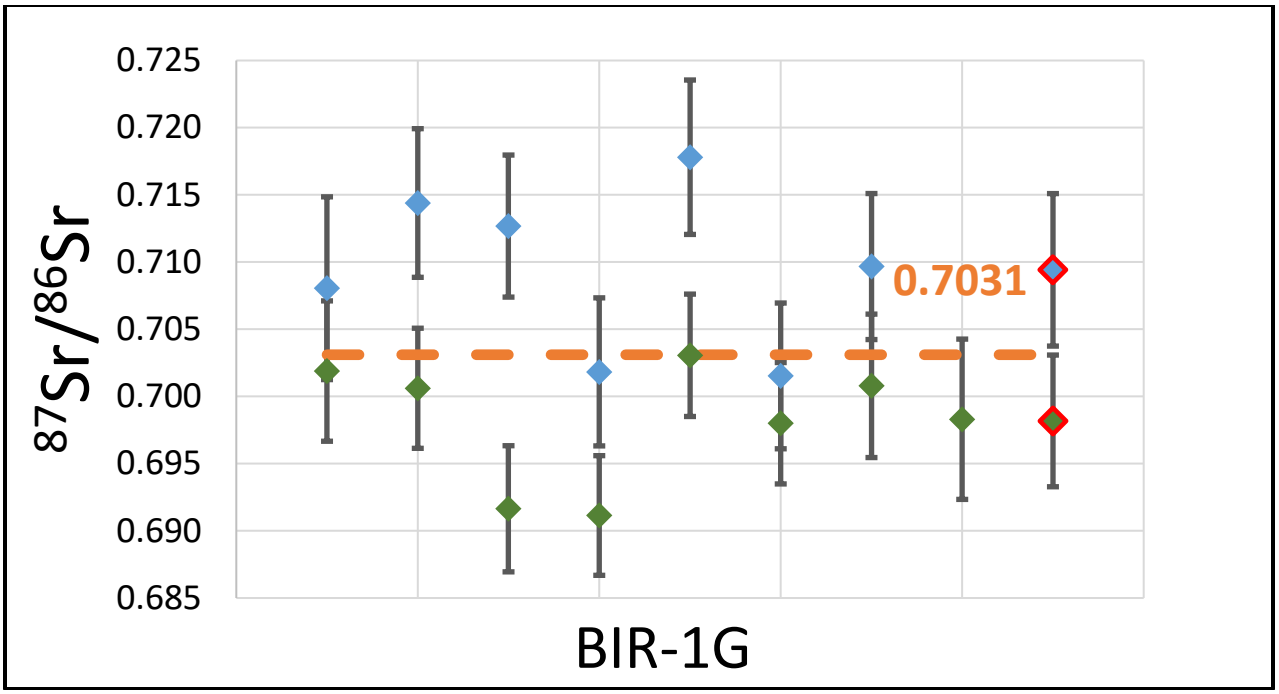

Figure 2a: Initial baseline test. 100 µm spot size, 10 ms dwell time. November analyses – light blue, January analyses – green. Average indicated in red border

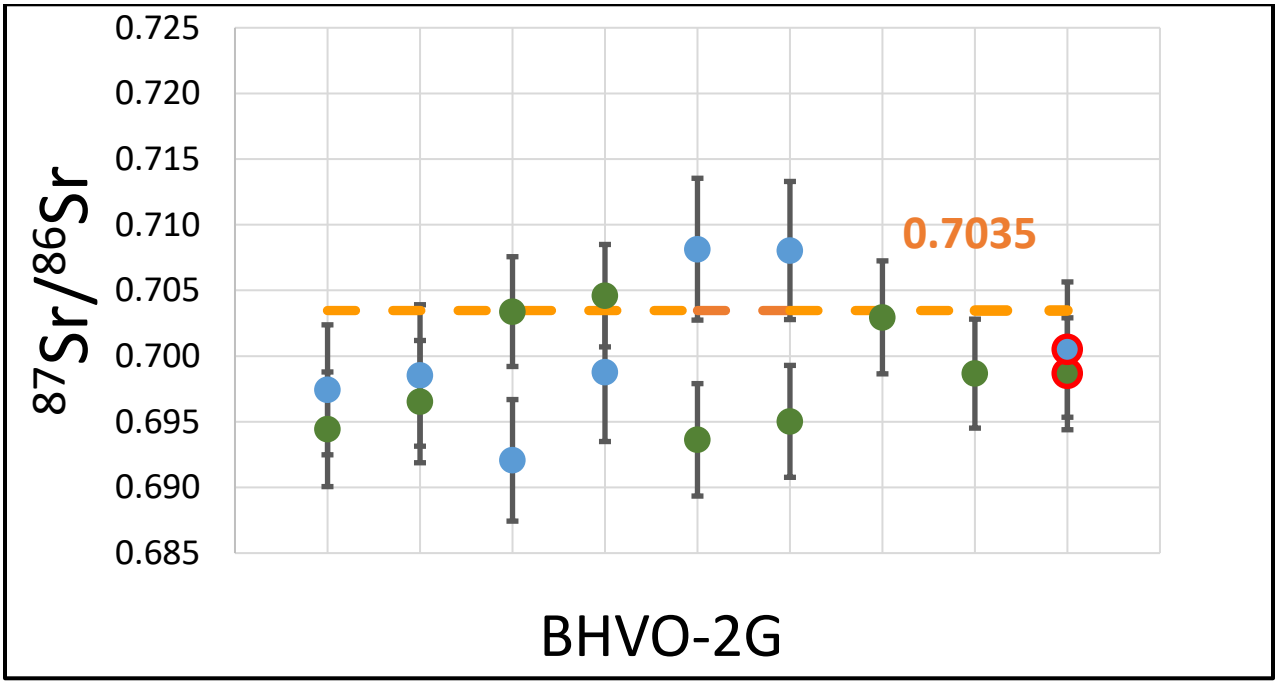

Figure 2b: Initial baseline test. 100 µm spot size, 10 ms dwell time. November analyses – light blue, January analyses – green. Average indicated in red border

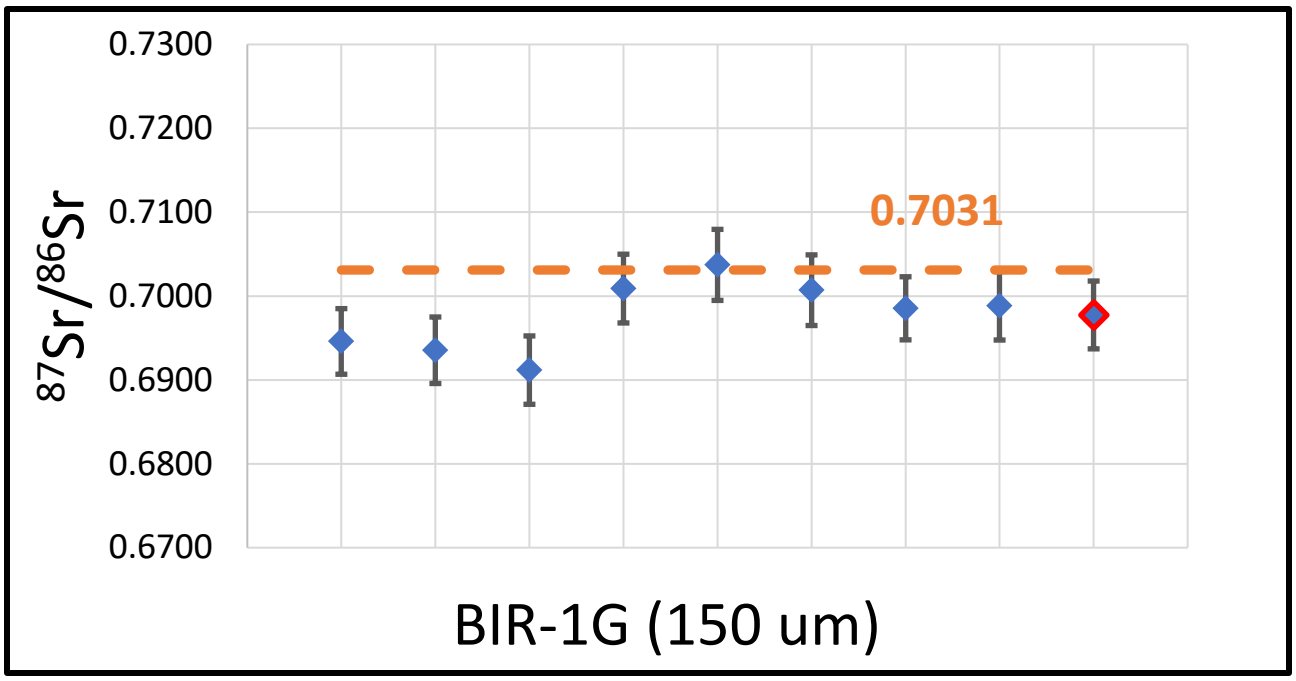

Figure 3b: January analyses with increased spot size (100 µm to 150 µm).

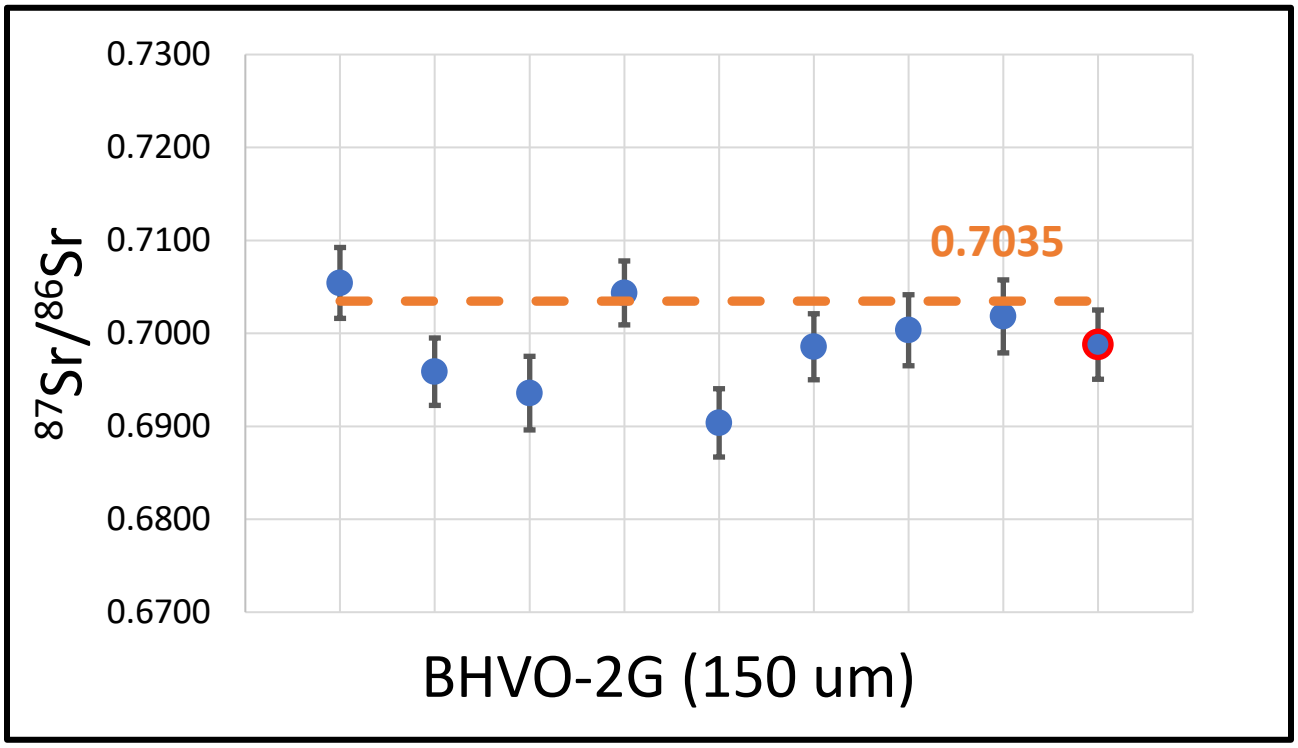

Figure 3a: January analyses with increased spot size (100 µm to 150 µm).

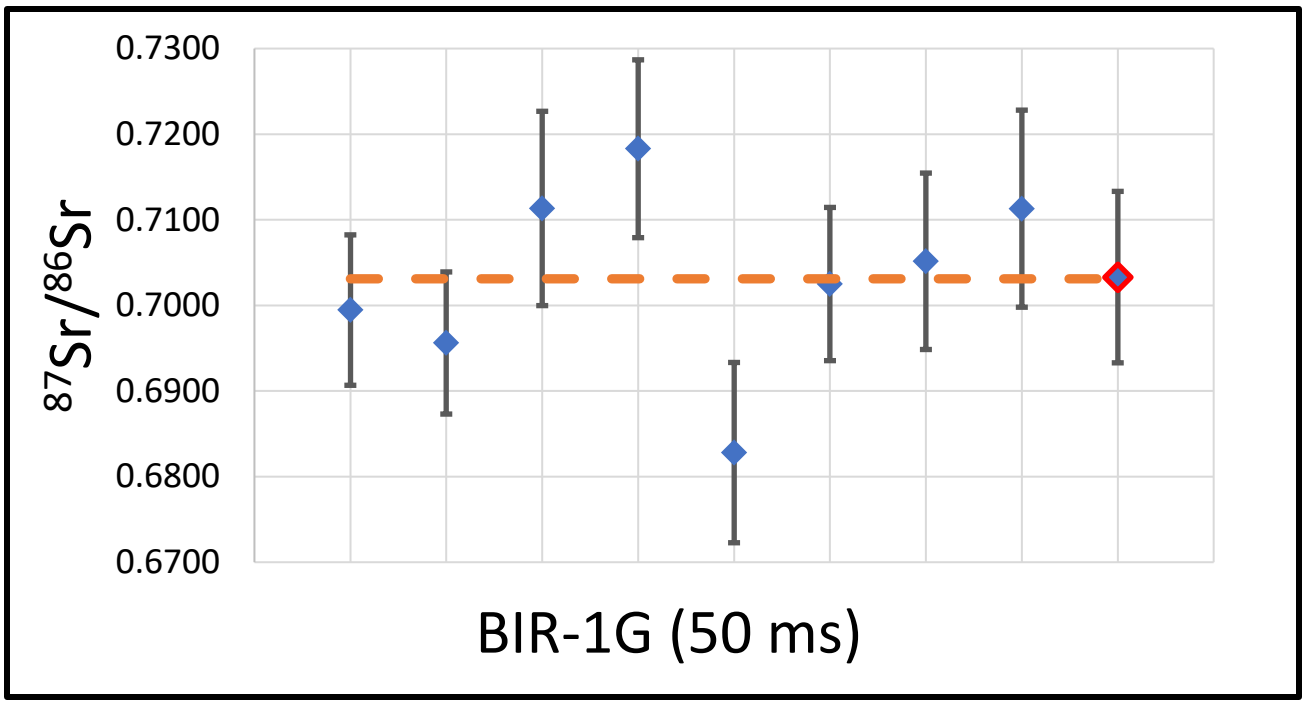

Figure 4a: January analyses with increased dwell time (10 ms to 50 ms).

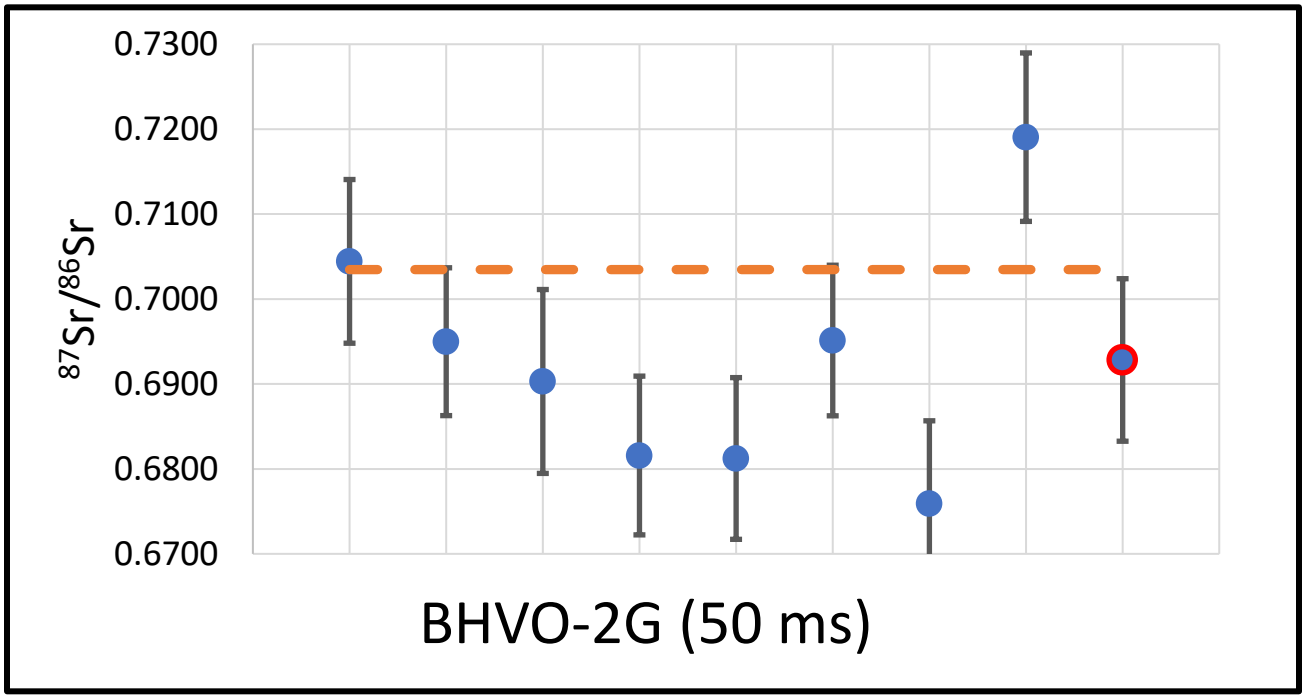

Figure 4b: January analyses with increased dwell time (10 ms to 50 ms).

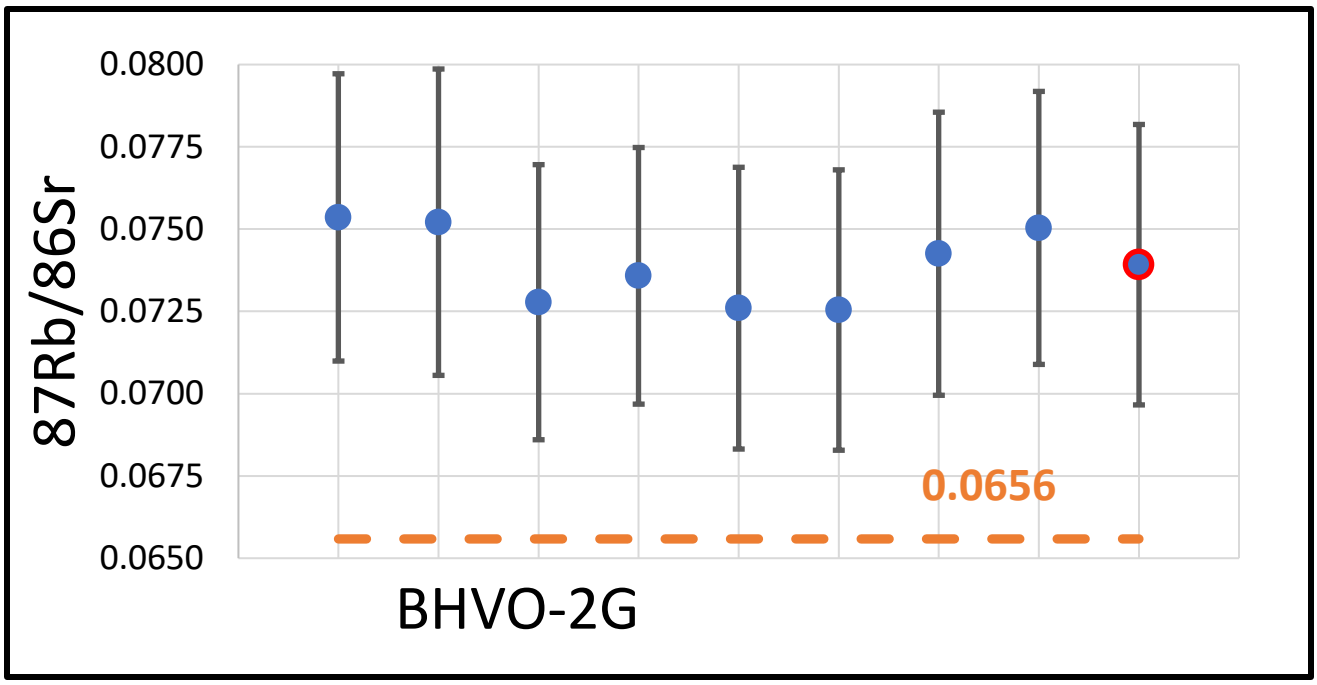

Figure 5a: January analyses $^{87}Rb/^{86}Sr$ ratios

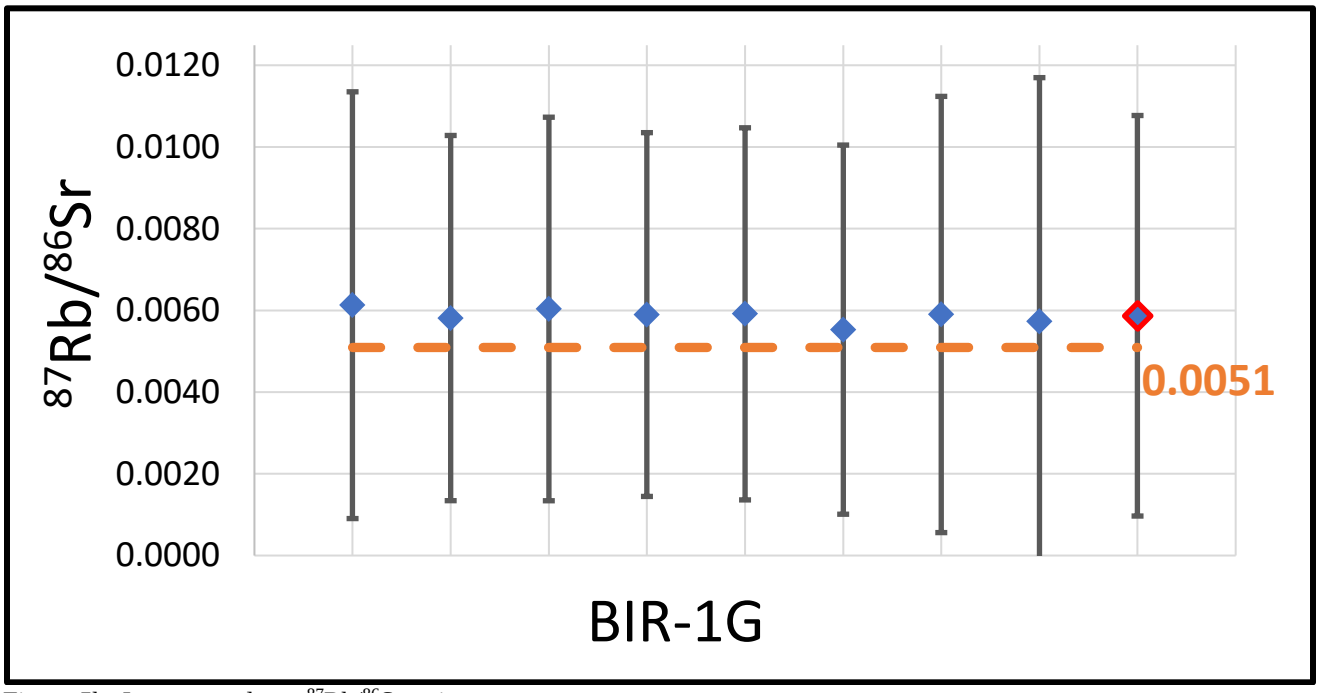

Figure 5b: January analyses $^{87}Rb/^{86}Sr$ ratios

IsoplotR Isochron Error

IsoplotR is an online software package that allows for the plotting of Rb-Sr isochrons with two data points or more. The settings used are Rb-Sr isochron, with 2 SEM % input errors, propagated external uncertainties, 2% $^{87}Sr/^{86}Sr$ and 15% $^{87}Rb/^{86}Sr$ ratio errors. The algorithm for the maximum likelihood regression model comes from York et. al 2004. Two data points with varying $^{87}Rb/^{86}Sr$ ratios are fit using the isochron equation for three ages of 4000 Ma, 2000 Ma, and 1000 Ma. The inputted $^{87}Rb/^{86}Sr$ and calculated $^{87}Sr/^{86}Sr$ ratios are entered into the IsoplotR interface and the resulting uncertainties are plotted (Figure 6). The initial $^{87}Rb/^{86}Sr$ data point for all calculation is 0.1. For all ages, 8 calculations were performed with the second $^{87}Rb/^{86}Sr$ data points at 1, 1.5, 2, 3, 5, 8, and 10. The initial $^{87}Rb/^{86}Sr$ data point of 0.1 was chosen to represent the generally basaltic crust of Mars (Ehlmann and Edwards 2014). The second data points were chosen to represent a spread of different minerals.

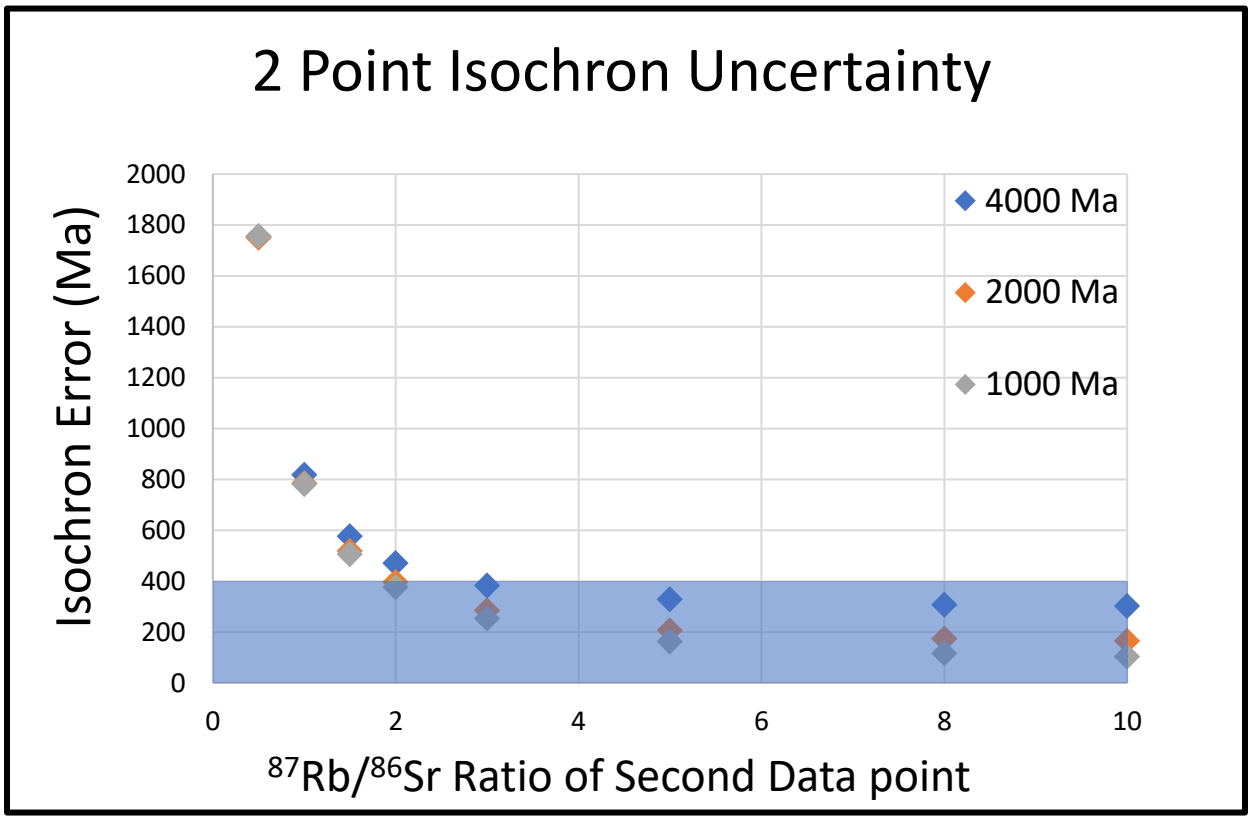

Figure 6: All initial $^{87}Rb/^{86}Sr$ data points are 0.1. The shaded blue marks the desired error of 400 Ma. Findings from ICPMS analyses are incorporated into calculation.

Discussion

Element Solution Experiments

The goal of the element solution experiments was to obtain production rates for the isobaric interferences and mass fractionation. On all the solutions besides Yb and Ho, there were significant interferences that made the production rates unreasonable. The production rate of Yb^{2+}/Yb^{+} and Ho^{2+}/Ho^{+} was approximately 0.15%, higher than originally expected but consistent for each of the isotopes measured. This production rate means a sample will need 10x the amount of REE as Rb or Sr for doubly charged ions to interfere with the analysis on a statistically significant level. The $^{87}Sr/^{86}Sr$ ratios for the two solutions of Sr and 1:1 Rb-Sr show that correcting for the ^{87}Rb overlap creates much higher uncertainty.

Solid Sample Analyses

The analysis of solid samples via LA provided a more representative production rate for the various isobars. The production rates obtained allowed for a threshold of counts per second (cps) to be calculated for where the interference becomes significant. With a low argide production rate of ~0.01%, if the ^{45}Sc count rate is less than 1000x that for ^{85}Rb or ^{88}Sr then the argide interference is below a measurable amount. The production rate of calcium dimers is ~0.004%, so if the cps of ^{44}Ca are less than 2500x the counts of ^{88}Sr then the interference is below statistically significant amount. The doubly charged heavy rare earth elements (Ho – Lu) pose a potentially greater problem to an accurate and precision measurement. The production rates for the doubly charged REE vary from ~10% to less than 1%. These rates are noticeably higher than observed by Jacobs (2015) whose rates were all below 1%, potentially due to the collision cell used by Jacobs (2015) or variance in plasma temperature. The caveat is that only a few isotopes impact a desired mass signal. The average production rate for these REE, based on data gathered at the University of Maryland, is between 2-4%. This is higher than the solution mode data gathered in fall 2019. The most abundant isotope for these elements is ^{174}Yb, ^{175}Lu, ^{180}Hf, ^{166}Er, and ^{164}Dy. ^{174}Yb. ^{166}Er, and ^{164}Dy. ^{174}Yb are the most important isotopes due to the mass signal they interfere with (82, 83 and 87). If the count rates (cps) for these isotopes are 3x less than the count rates (cps) for mass 87, mass 83, and mass 82 then the interference will be below a statistically significant amount.

BIR-1G and BHVO-2G

The analyses of BIR-1G and BHVO-2G showed that accuracy for $^{87}Sr/^{86}Sr$ ratios are within 2% and uncertainties within 2% (2SEM) and are reproducible. Of the two laser parameters explored, increasing the spot size from 100 um to 150 um produced similar results, suggesting that the count rate is not the limited factor in the precision of our measurements. The increased dwell time cause a noticeable increase in uncertainty, likely reflecting the greater impact of flicker noise and time-varying plasma conditions at longer timescales. Correction methods 2, 3 and 4 produced the same accuracy and precision as the 1^{st} method. This may be due to low counts of Rb.

IsoplotR Isochron Error

The results from the IsoplotR calculations are promising. With the current Rb/Sr measurement accuracies, it is possible to construct an accurate two-point isochron given sufficient $^{87}Rb/^{86}Sr$ spread for sample ages 1-4 Ga. Multi-point (more than two data points)

isochrons and/or reducing the uncertainty of the $^{87}Rb/^{86}Sr$ measurements could improve the errors (Table 5). By combining the IsoplotR results and the ability to accurately measure Rb/Sr ratios with LA-ICPMS, accurate *in situ* radiometric age determination measurements via LA-ICPMS on Mars are feasible. It is important to consider that the 2% and 15% errors for $^{87}Sr/^{86}Sr$ and $^{87}Rb/^{86}Sr$ ratios were derived from the analysis of basaltic sample materials; thus, these figures of merit may change based on sample mineralogy. Minimizing the uncertainty on $^{87}Rb/^{86}Sr$ ratio measurements is a priority for future research. Obtaining lower uncertainties may be possible on higher abundance Rb samples, or through different data treatment. Also, the data points for the isochron are fit with their respective age which for natural samples can be affected based on the mobility of Rb or Sr within mineral phases.

Data Point	$^{87}Rb/^{86}Sr$	$^{87}Sr/^{86}Sr$	Age (Ma)	Isochron Error	
Point 1	0.1	0.7047	4000	180	4.5%
Point 2	1	0.7565			
Point 3	2	0.8139			
Point 4	5	0.9864			

Table 5: IsoplotR isochron error using $^{87}Rb/^{86}Sr$ error = 5% (2σ) and $^{87}Sr/^{86}Sr$ error = 2% (2σ).

Conclusion

The goal of this study was to evaluate the ability of LA-ICPMS for Rb-Sr chronological applications. The solution mode experiment estimated the potential interference from doubly charged REE but did not enable the characterization of production rates of the other isobars. The solid sample analyses further quantified the doubly charged REE and succeeded in estimating the other isobars (excluded zinc oxides). The BIR-1G and BHVO-2G analyses demonstrated that accurate Sr ratios can be achieved, using Kr, Rb and mass fractionation corrections via LA-ICPMS, with this technology. This project is intended to be a baseline test to understand the feasibility of applying this method to a future spaceflight mission. *In-situ* measurements taken by a spaceflight instrument will likely suffer from reduced accuracy and precision when compared to a terrestrial lab. This must be taken into considered when evaluating the estimated isochron error. Based on the information gathered, achieving the desired accuracy and precision is viable.

Future Work

Further analyses and research need to be conducted to constrain the overall accuracy and precision of an isochron age. Analyzing standard reference materials with higher Rb/Sr ratios will provide insight into how varying levels of Rb will impact the accuracy and precision of the measurements. Dr. McDonough has incorporated an interquartile range filter and moving averages into the data treatment. These techniques have been shown to reduce the uncertainty. Processing all the analyses of BHVO-2G and BIR-1G through this method will help determine an improved correction method. Continued calculations using IsoplotR with expected Martian Rb/Sr ratios can help further prove feasibility of constructing an accurate isochron from *in situ* measurements. An important step in the overall process of this project is to construct an isochron from a natural sample. Using a sample that has been dating by means of Rb-Sr will allow a comparison of accuracy and precision. The work done so far provides a foundation for continued research.

References

Arevalo, R. 2014. “Laser Ablation ICP-MS and Laser Fluorination GS-MS.” *Treatise on Geochemistry*, pp. 425–441., doi:10.1016/b978-0-08-095975-7.01432-7

Cohen, B.A., Malespin, C.A., Farley, K.A., Martin, P.E., Cho, Y., Mahaffy, P.R. 2019. “In Situ Geochronology on Mars and the Development of Future Instrumentation.” *Astrobiology*, vol. 19, no. 11, 2019, pp. 1303–1314., doi:10.1089/ast.2018.1871.

Dickin, A.P. 2005. *Radiogenic Isotope Geology*. Cambridge University Press.

Ehlmann, B.L., and Edwards, C.S. 2014. “Mineralogy of the Martian Surface.” Annual Review of Earth and Planetary Sciences, vol. 42, no. 1, pp. 291–315., doi:10.1146/annurev-earth-060313-055024.

“Isotopic Compositions of the Elements 2013 (IUPAC Technical Report).” *Chemistry International*, vol. 38, no. 3-4, 2016, doi:10.1515/ci-2016-3-415.

Jacobs, J.L. 2015. “Diagnostic Studies of Ion Beam Formation in Inductively Coupled Plasma Mass Spectrometry with the Collision Reaction Interface.” doi:10.31274/etd-180810-4400.

Jenner, F.E., and Arevalo, R.D. 2016. “Major and Trace Element Analysis of Natural and Experimental Igneous Systems Using LA–ICP–MS.” *Elements*, vol. 12, no. 5, pp. 311–316., doi:10.2113/gselements.12.5.311.

Jochum, K. P., Willbold, M., Raczek, I., Stoll, B., Herwig, K. 2007. “Chemical Characterisation of the USGS Reference Glasses GSA-1G, GSC-1G, GSD-1G, GSE-1G, BCR-2G, BHVO-2G and BIR-1G Using EPMA, ID-TIMS, ID-ICP-MS and LA-ICP-MS.” *Geostandards and Geoanalytical Research*, vol. 29, no. 3, pp. 285–302., doi:10.1111/j.1751-908x.2005.tb00901.x.

Jochum, K. P., Stoll, B., Weis, U., Kuzmin, D. V. and Sobolev, A. V. 2009. “In Situ Sr Isotopic Analysis of Low Sr Silicates Using LA-ICP-MS.” *Journal of Analytical Atomic Spectrometry*, vol. 24, no. 9, p. 1237., doi:10.1039/b905045k.

National Aeronautics and Space Administration. 2015. *NASA Technology Roadmaps, TA8: Science Instruments, Observatories, and Sensor Systems.* https://www.nasa.gov/sites/default/files/atoms/files/2015_nasa_technology_roadmaps_ta_8_science_instruments_final.pdf

Olesik, J.W. 2014. “Inductively Coupled Plasma Mass Spectrometers.” *Treatise on Geochemistry*, pp. 309–336., doi:10.1016/b978-0-08-095975-7.01426-1.

Robbins, S.J., 2014. “New Crater Calibrations for the Lunar Crater-Age Chronology.” *Earth and Planetary Science Letters*, vol. 403, pp. 188–198., doi:10.1016/j.epsl.2014.06.038.

Vroon, P. Z., van der Wagt, B., Koornneef, J. M., Davies, G. R. 2008. “Problems in Obtaining Precise and Accurate Sr Isotope Analysis from Geological Materials Using Laser Ablation MC-ICPMS.” *Analytical and Bioanalytical Chemistry*,390, 2, 465–476, doi:10.1007/s00216-007-1742-9.

York, D., and Evensen, N.M. 2004. “Unified Equations for the Slope, Intercept, and Standard Errors of the Best Straight Line.” *American Journal of Physics*, vol. 72, no. 3, pp. 367–375., doi:10.1119/1.1632486.

Appendix - Element Menus

Sr only solution

	[min:sec:ms]	[h:min:sec]		
Low	00 : 00 : 024	00 : 00 : 49	Runs/Passes (Meas.) :	2000 * 1 + 0 * 0 + 0 * 0
Med.	00 : 00 : 000	00 : 00 : 00	Runs/Passes (Eval.) :	2000 * 1 + 0 * 0 + 0 * 0
High	00 : 00 : 000	00 : 00 : 00	Res. Switch Delay [s] :	2
	Total Time	00 : 00 : 49		

Entry	Locked	Isotope	Calib Threshold	Accurate Mass	Method Mass Offset	Mass Window	Mass Range	Magnet Mass	Settling Time
Low									
1	No	Sr84	0	83.9129	0.0000	1	83.911 - 83.914	83.913	0.001
2	No	Sr86	0	85.9087	0.0000	1	85.907 - 85.910	83.913	0.001
3	No	Sr87	0	86.9084	0.0000	1	86.907 - 86.910	83.913	0.001
4	No	Sr88	0	87.9051	0.0000	1	87.904 - 87.907	83.913	0.001

	[min:sec:ms]	[h:min:sec]		
Low	00 : 00 : 024	00 : 00 : 49	Runs/Passes (Meas.) :	2000 * 1 + 0 * 0 + 0 * 0
Med.	00 : 00 : 000	00 : 00 : 00	Runs/Passes (Eval.) :	2000 * 1 + 0 * 0 + 0 * 0
High	00 : 00 : 000	00 : 00 : 00	Res. Switch Delay [s] :	2
	Total Time	00 : 00 : 49		

Entry	Locked	Isotope	Sample Time	Samples per Peak	Segment Duration	Search Window	Integration Window	Scan Type	Detection Mode
Low									
1	No	Sr84	0.0050	1	0.005	150	80	EScan	Counting
2	No	Sr86	0.0050	1	0.005	150	80	EScan	Counting
3	No	Sr87	0.0050	1	0.005	150	80	EScan	Counting
4	No	Sr88	0.0050	1	0.005	150	80	EScan	Counting

1:1 Rb-Sr solution

	[min:sec:ms]	[h:min:sec]		
Low	00 : 00 : 030	00 : 01 : 01	Runs/Passes (Meas.) :	2000 * 1 + 0 * 0 + 0 * 0
Med.	00 : 00 : 000	00 : 00 : 00	Runs/Passes (Eval.) :	2000 * 1 + 0 * 0 + 0 * 0
High	00 : 00 : 000	00 : 00 : 00	Res. Switch Delay [s] :	2
	Total Time	00 : 01 : 01		

Entry	Locked	Isotope	Calib Threshold	Accurate Mass	Method Mass Offset	Mass Window	Mass Range	Magnet Mass	Settling Time
Low									
1	No	Sr84	0	83.9129	0.0000	1	83.911 - 83.914	83.913	0.001
2	No	Rb85	0	84.9113	0.0000	1	84.910 - 84.913	83.913	0.001
3	No	Sr86	0	85.9087	0.0000	1	85.907 - 85.910	83.913	0.001
4	No	Sr87	0	86.9084	0.0000	1	86.907 - 86.910	83.913	0.001
5	No	Sr88	0	87.9051	0.0000	1	87.904 - 87.907	83.913	0.001

	[min:sec:ms]	[h:min:sec]		
Low	00 : 00 : 030	00 : 01 : 01	Runs/Passes (Meas.) :	2000 * 1 + 0 * 0 + 0 * 0
Med.	00 : 00 : 000	00 : 00 : 00	Runs/Passes (Eval.) :	2000 * 1 + 0 * 0 + 0 * 0
High	00 : 00 : 000	00 : 00 : 00	Res. Switch Delay [s] :	2
	Total Time	00 : 01 : 01		

Entry	Locked	Isotope	Sample Time	Samples per Peak	Segment Duration	Search Window	Integration Window	Scan Type	Detection Mode
Low									
1	No	Sr84	0.0050	1	0.005	150	80	EScan	Counting
2	No	Rb85	0.0050	1	0.005	150	80	EScan	Counting
3	No	Sr86	0.0050	1	0.005	150	80	EScan	Counting
4	No	Sr87	0.0050	1	0.005	150	80	EScan	Counting
5	No	Sr88	0.0050	1	0.005	150	80	EScan	Counting

BIR-1G and BHVO-2G

	[min:sec:ms]	[h:min:sec]		
Low	00 : 00 : 099	00 : 01 : 10	Runs/Passes (Meas.) :	700 * 1 + 0 * 0 + 0 * 0
Med.	00 : 00 : 000	00 : 00 : 00	Runs/Passes (Eval.) :	700 * 1 + 0 * 0 + 0 * 0
High	00 : 00 : 000	00 : 00 : 00	Res. Switch Delay [s] :	2
	Total Time	00 : 01 : 10		

Entry	Locked	Isotope	Calib Threshold	Accurate Mass	Method Mass Offset	Mass Window	Mass Range	Magnet Mass	Settling Time
Low									
1	No	Se77	0	76.9194	0.0000	1	76.918 - 76.921	76.919	0.001
2	No	Se78	0	77.9168	0.0000	1	77.915 - 77.918	76.919	0.001
3	No	Kr82	0	81.9129	0.0000	1	81.912 - 81.914	76.919	0.001
4	No	Kr83	0	82.9136	0.0000	1	82.912 - 82.915	76.919	0.001
5	No	Sr84	0	83.9129	0.0000	1	83.911 - 83.914	76.919	0.001
6	No	Rb85	0	84.9113	0.0000	1	84.910 - 84.913	76.919	0.001
7	No	Sr86	0	85.9087	0.0000	1	85.907 - 85.910	76.919	0.001
8	No	Sr87	0	86.9084	0.0000	1	86.907 - 86.910	76.919	0.001
9	No	Sr88	0	87.9051	0.0000	1	87.904 - 87.907	76.919	0.001

	[min:sec:ms]	[h:min:sec]		
Low	00 : 00 : 099	00 : 01 : 10	Runs/Passes (Meas.) :	700 * 1 + 0 * 0 + 0 * 0
Med.	00 : 00 : 000	00 : 00 : 00	Runs/Passes (Eval.) :	700 * 1 + 0 * 0 + 0 * 0
High	00 : 00 : 000	00 : 00 : 00	Res. Switch Delay [s] :	2
	Total Time	00 : 01 : 10		

Entry	Locked	Isotope	Sample Time	Samples per Peak	Segment Duration	Search Window	Integration Window	Scan Type	Detection Mode
Low									
1	No	Se77	0.0100	1	0.010	150	80	EScan	Counting
2	No	Se78	0.0100	1	0.010	150	80	EScan	Counting
3	No	Kr82	0.0100	1	0.010	150	80	EScan	Counting
4	No	Kr83	0.0100	1	0.010	150	80	EScan	Counting
5	No	Sr84	0.0100	1	0.010	150	80	EScan	Counting
6	No	Rb85	0.0100	1	0.010	150	80	EScan	Counting
7	No	Sr86	0.0100	1	0.010	150	80	EScan	Counting
8	No	Sr87	0.0100	1	0.010	150	80	EScan	Counting
9	No	Sr88	0.0100	1	0.010	150	80	EScan	Counting